ACS OMEGA

Open Access

http://pubs.acs.org/journal/acsodf

Article

Strategically Designed Ternary Nanohybrids of Titanate Nanosheet and Polydopamine-Coated Carbon Nanotubes for Highly Efficient Enrichment of Uranium(VI)

Zhiyang Jiang, Yuzhi Zhou,* Wenshuo Wang, Zheng Yin, Mingze Zhao, Lei Yu, Sijie Ren, Han Xiao, and Yanfang Ma

Cite This: *ACS Omega* 2024, 9, 49108−49120

Read Online

ACCESS | Metrics & More | Article Recommendations | Supporting Information

ABSTRACT: A strategically designed ternary nanohybrid (TNS-PDA/CNT), consisting of titanate nanosheet (TNS) and polydopamine-modified multiwalled carbon nanotube (PDA/CNT composite), was synthesized by the facile hydrothermal method and wet impregnation method for removal of U(VI) from aqueous solution and were characterized by transmission electron microscopy (TEM), scanning electron microscopy−energy-dispersive X-ray spectroscopy (SEM-EDS), X-ray diffraction (XRD), Fourier transform infrared (FT-IR), thermogravimetric analysis (TGA), Raman spectroscopy, Brunauer−Emmett−Teller (BET), and X-ray photoelectron spectroscopy (XPS). TNSs were introduced into the PDA/CNT composite, which effectively averted the agglomeration of the CNT and further exposed more adsorption sites. PDA thin layer exposing more active sites was conducive to enhance adsorption capacity and kinetic. The adsorption process was largely influenced by pH values and weakly affected by ionic strength, indicating that the adsorption process was controlled by inner-sphere surface complexes because of TNS-PDA/CNT with multiple functional groups, including imine, catechol, amine, and hydroxyl groups. The isotherm data could be well described by the Langmuir model, and the monolayer maximum adsorption was determined to be 309.60 mg/g at pH = 5.0 and temperature = 45 °C. Thermodynamic parameters ($\Delta G^\circ < 0$, $\Delta S^\circ > 0$, and $\Delta H^\circ < 0$) showed that the nature of adsorption was endothermic and spontaneous. By XRD, FT-IR, and XPS analyses, the adsorption mechanism mainly involved surface complexation and ion exchange. In summary, the TNS-PDA/CNT materials are fully qualified as a satisfactory adsorbent for the purification and recovery of U(VI) from wastewater.

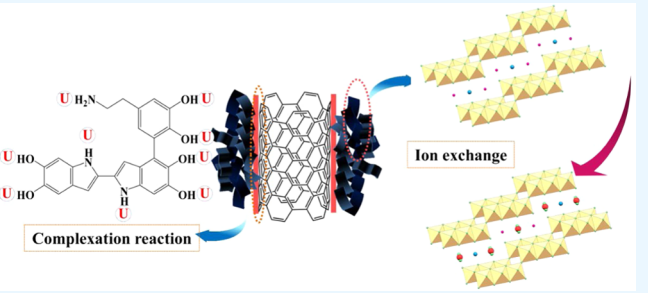

INTRODUCTION

With the global warming problem becoming increasingly prominent, the proportion of conventional energy use is under control, and new energy has gradually become a new star in the global energy market, such as wind energy, solar energy, and tidal energy.[1] Nuclear energy has widely been perceived as the most important component of modern energy system because of low carbon, clean, sustainable, and stable power supply, and generated about 10.6% of the world's electricity in 2013 and 5.7% of the world's energy. Radioactive uranium has dual attributes, both an essential nuclear fuel and a significant fraction of the wastewater.[2] Thus, from resource recovery as well as environmental protection, the preconcentration and enrichment of uranium from nuclear effluent become extremely imperative. In recent years, A diverse array of technologies has been employed for the extraction of radionuclides from water-based, such as oxidation/reduction, coprecipitation,[3] ion exchange,[4] and electrodeposition.[5] Of varied methods, adsorption is perceived to be an extensively used and financially viable strategy because of its simple handling, wide adaptation range, and high removal rate. Although a variety of adsorbents, including zero/two-dimensional (0D/2D) C_4N/C_6N_7 homostructure hybrids,[6] layered metal sulfides,[7] multiwalled carbon nanotubes,[8] montmorillonite,[9] etc. have been developed for removal of various pollutants, the adsorbents are subjected to its shortcomings either poor adsorption selectivity or low adsorption capacity, which greatly restrict its application. Therefore, it is imperative to design economical and efficient U(VI)-retaining adsorbents for coping with challenges in water remediation.

Carbon nanotubes, since their discovered by Iijima in 1991,[10] have attracted a great deal of interest in multiple fields and have been extensively studied as a promising adsorbent alternative for the removal of heavy metals[11,12] and radio-

Received: June 4, 2024
Revised: November 22, 2024
Accepted: November 22, 2024
Published: December 5, 2024

nuclides[13,14] from polluted waters because of their prominent thermal and radiation resistance and favorable chemical stability in highly acidic media.[15] However, owing to potent van der Waals forces, unmodified carbon nanotubes exhibit hydrophobic properties and are prone to forming bulky aggregates in waterbody, and the adsorption capacity and selectivity of carbon nanotubes are also poor because of lack of functional groups.[16] The inherent disadvantages greatly restrict its application. Therefore, surface modification of carbon nanotubes (CNT) by grafting functional groups or attaching suitable nanostructures on the nanotubes will be a very wise strategy to improve their application.[17,18]

Polydopamine (PDA), an eco-friendly biopolymer, has garnered considerable attention in environmental preservation due to its plethora of functional groups (such as imine/amine and catechol), its strong adhesive properties (akin to adhesion proteins secreted by mussels), and the simplicity of its synthesis conditions.[19] The merits, on the one hand, achieve the tight connection and compatibility between PDA and almost any solid material surface, on the other hand, provide a great quantity of adsorption site to bind with heavy metal ions.[20,21] Consequently, PDA's adaptability positions it as an auspicious candidate for capturing U(VI) from contaminated water. Nevertheless, PDA tends to aggregate into irregular micro- or nanoscale clusters during the self-polymerization process, which reduces the surface areas and permeability, limits the accessibility of active sites,[22,23] and ultimately limits its application. To address this limitation, numerous strategies have been employed to unveil more active sites and increase the specific surface area through the application of PDA coatings on substrates with large surface areas, such as α-MnO_2 and activated carbon,[24] and activated carbon[25] and *Aspergillus niger* microspheres.[26]

Titanate nanomaterial, first synthesized by German scientist Kasuga,[27,28] has attracted great interest due to its prominent characteristics, including high surface area, unique layered structure, and excellent ion exchange capacity, and be extensively employed to remove organic pollutants and heavy metals from complex natural water.[29−31] For example, Liu et al.[29] reported an efficient adsorbent of multilayer titanate nanotubes with satisfactory adsorption capacity. Sheng et al.[32] explored the adsorption performance of titanate nanotubes for capturing U(VI) ions and found the promoting effect of humic acid on U(VI) ions adsorption. Moreover, titanate nanosheet (TNS) as a metastable layered structure has the advantages of larger specific area and thinner thickness than other morphology, such as tubular, rod, and fibrous, which can provide more binding sites for capturing U(VI). However, TNSs have inherent shortcomings of easy-to-form aggregates after hydrated and lack of functional groups, which greatly limit their application. Therefore, attaching TNS to the CNT surface can be expected.

Taking the advantages of CNT, PDA, and TNS, we attempted to fabricate a hierarchical nanomaterial (TNS-PDA/CNT) by a layer-by-layer (LBL) technique. Namely, polydopamine coating layers were evenly distributed on CNTs surface by a simple impregnation method, followed by in situ growth of TNS on PDA-modified CNT via a mild hydrothermal method. In this study, TNS-PDA/CNT as a U(VI) scavenger was employed to systematically evaluate the influence of environmental conditions on adsorption performance, such as pH, humic acid (HA), ionic strength, reaction time, temperature, coexisting ions, and initial concentration. More so, the possible adsorption mechanism was carefully explored by Fourier transform infrared (FTIR), X-ray diffraction (XRD), and X-ray photoelectron spectroscopy (XPS).

2. EXPERIMENTAL SECTION

2.1. Materials and Chemicals. Multiwall carbon nanotubes (CNT: purity >95%, outer diameter 30−50 nm, length 10−30 μm) were purchased from the Chengdu Institute of Organic Chemistry of the Chinese Academy of Science. Tris−HCl and dopamine hydrochloride (purity >98%) were purchased from Sigma-Aldrich Chem. Tetrabutyl titanate and sodium hydroxide were obtained from Tianjin Kermel Reagent Co., Ltd. All reagents and chemicals were of analytical grade unless otherwise noted.

2.2. Synthesis of TNS-PDA/CNT. 0.5 g of CNT (0.5 g) was added to 200 mL beakers containing 80 mL of absolute ethanol and 60 mL of ultrapure water. The mixtures were ultrasonicated for 30 min followed by 5 min of stirring at ambient temperature. Subsequently, 300 mg of dopamine hydrochloride was added to the mixture, and then 20 mL of 35 mM Tris was added dropwise with continuous stirring to the above mixture. After a polymerization reaction of 6 h, the precipitate resulted in collection by centrifugation and was dried at 60 °C.

The TNS-PDA/CNT synthesis was performed in two steps. In the first step, $Ti(OH)_x$ was uniformly attached to PDA/CNT surfaces to form the nanocomposite $Ti(OH)_x$-PDA/CNT. Well-washed PDA/CNT was placed in 200 mL of ethanol and 2 mL of distilled water and dispersed for 30 min using an ultrasonicator, followed by 30 min of stirring at room temperature to form a homogeneous mixture, denoted as A solution. 8 mL of tetrabutyl titanate was dispersed well in 20 mL of ethanol and denoted as B solution. Then, B solution was added dropwise into A solution under strong stirring at 80 °C. After stirring for 100 min, the $Ti(OH)_x$-PDA/CNT composite was separated through centrifugation and rinsed with distilled water. In the following stage, 1.2 g of the $Ti(OH)_x$-PDA/CNT composite was dispersed in 80 mL of a 10 M NaOH solution and stirred continuously for 6 h.

2.3. Batch Adsorption of U(VI). U(VI) adsorption experiments were performed in batch-shaking method and were done concretely by mixing 0.01 g of adsorbents with 50 mL of U(VI) solution (20 mg/L). The mixture was then shaken at 25 °C and 200 rpm. After adsorption, solid−liquid separation was carried out through a syringe filter (0.22 μm), and the solution obtained was analyzed by a visible spectrophotometer (Thermo Evolution 300) at λ = 652 nm. The adsorption capacity (q_e, mg/g), removal percentage (R, %), and solid phase distribution coefficient (K_d, mL/g) were calculated by eqs 1−3.

$$R\ (\%) = \frac{C_0 - C_e}{C_0} \times 100 \tag{1}$$

$$q_e = \frac{V(C_0 - C_e)}{W} \tag{2}$$

$$K_d = \frac{C_0 - C_e}{C_e} \times \frac{V}{W} \tag{3}$$

where C_0 and C_e (mg/L) denote the initial and equilibrium concentrations, respectively, q_e (mg/g) represents the

https://doi.org/10.1021/acsomega.4c05253
ACS Omega 2024, 9, 49108−49120

adsorbed radionuclide quantity per gram of TNS-PDA/CNT, V (mL) indicates the solution volume, and W (g) refers to the adsorbent weight.

2.4. Characterization Techniques. The crystal structure of the TNS-PDA/CNT samples was analyzed by using X-ray diffraction (XRD) patterns, acquired with a D8-advance X-ray diffractometer (Bruker, Germany) using Cu Kα radiation. The surface morphology and structure of the TNS-PDA/CNT were recorded by scanning electron microscopy (SEM, JEOL 7800F, Japan) and transmission electron microscopy (TEM, JEM-F200, Japan). Element composition and chemical state alterations were examined by X-ray photoelectron spectroscopy (XPS) and C 1s signal at 284.8 eV served as a reference. FTIR spectra of the TNS-PDA/CNT samples were recorded on an Avatar 360 FT-IR spectrophotometer (Nicolet, Waltham, MA) ranging from 4000 to 400 cm^{-1}. The textural properties of the adsorbents were identified by the N_2 adsorption−desorption isotherms, and the pore size distributions were measured by Barrett−Joyner−Halenda (BJH). TGA was characterized by STD 600 (TA Instruments) under a nitrogen atmosphere from 25 to 1000 °C at a heating rate of 10 °C/min.

2.5. Adsorption Models. The pseudo-first-order and pseudo-second-order models were used to study the adsorption kinetic. The Langmuir, Freundlich, and Temkin isotherm models were used to fit the experimental data for the adsorption isotherm. And the specific information is presented in Supporting Information Sections 1 and 2.

3. RESULTS AND DISCUSSION

3.1. Characterization of TNS-PDA/CNT. The TEM images of CNT, Ti(OH)$_x$-PDA/CNT, and TNS-PDA/CNT are shown in Figure 1. The pure CNT appeared interwoven and displayed a hollow tubular structure with an inner diameter of ca. 5−6 nm and an outer diameter of 20−25 nm due to strong van der Waals force (Figure 1a). The agglomerated component attached to the surface of PDA/CNT can also be observed in Figure 1b, which proves the presence of the Ti-based layer. The TNS-PDA/CNT composites present CNT embedded in irregular sheets of TNS in the TEM and SEM (Figure 1c), in which the nanotubular structure of CNT remains unchanged. Also, the high-resolution TEM (HRTEM) image showed that the value of the d-spacing was 0.81 nm in accordance with the d spacing of the 020 planes in sodium titanate.[33] The EDS line scanning and face scanning results of TNS-PDA/CNT showed that the material was composed of carbon, nitrogen, titanium, sodium, and oxygen, which directly confirmed the successful hybridization of CNT, PDA, and TNS (see Supporting Information Figures S1 and S2). However, the presence of U element in the spectrum of U-TNS-PDA/CNT demonstrated that the U(VI) ions were successfully trapped by TNS-PDA/CNT(see Supporting Information Figure S3).

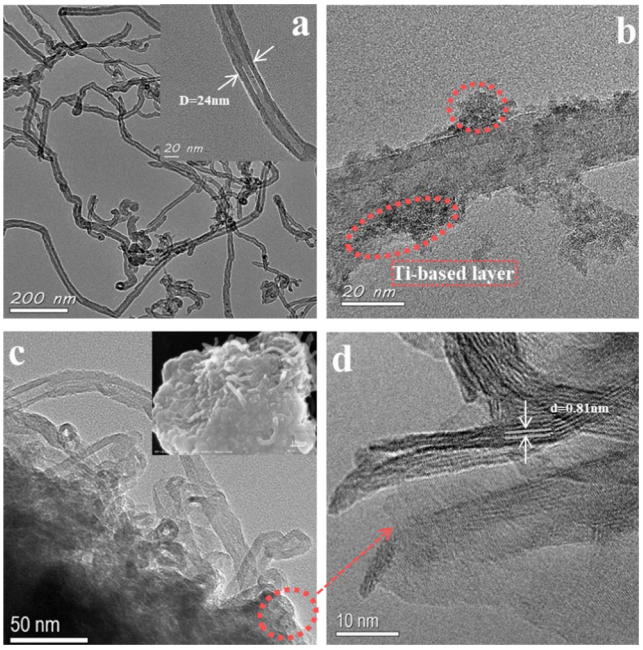

Figure 1. TEM images of (a) CNT, (b) Ti(OH)x-PDA/CNT, and (c) TNS-PDA/CNT; (d) high-resolution TEM (HRTEM) images of TNS-PDA/CNT.

To discern the phase structure of the TNS-PDA/CNT composite, the as-synthesized nanocomposites were characterized by XRD (Figure 2a). For CNT, the intensive peaks at 2θ = 26.09 and 43.09° corresponded to the graphite structure (002) and (100) planes of the CNT.[34] After PDA coating, the characteristic peaks of CNT remained, but the intensity of peaks slightly decreased, which implied that PDA coating was amorphous and the phase structure of the pristine CNT was not destroyed during the PDA coating. In the XRD pattern of Ti(OH)$_x$-PDA/CNT, some new peaks were observed at 2θ = 38.0°, 48.0, and 54.2, which could be attributed to the formation of intermediate components (Ti(OH)$_x$). After the alkaline hydrothermal reaction of Ti(OH)$_x$-PDA/CNT, XRD pattern exhibited the characteristic absorption bands of $Na_2Ti_3O_7$ at 2θ= 8.69, 24.7, 26.9, and 48.2°, corresponding to crystal indexes of (200), (110), (310), and (020), respectively, and implied the successful convention transformation from Ti(OH)$_x$ to $Na_2Ti_3O_7$.[35] In addition, the first peak position at 8.69° reflected the interlayer space of $Na_2Ti_3O_7$, which was calculated to be d_{100} = 0.86 nm by Bragg's law.

For confirmation of CNT functionalization, FTIR analysis was carried out and the recorded spectra are presented in Figure 2b,c. For pure CNT, the adsorption peaks at 1634 and 1578 cm^{-1} were attributed to the stretching vibrations of C=C.[36] The strong band around 3432 cm^{-1} was associated with the O−H stretching vibration. In the spectra of PDA/CNT, some new peaks appeared at 1616 cm^{-1} (the stretching vibration of aromatic ring and bending ring vibration of N−H),[6] 1519 cm^{-1} (the shearing vibration of N−H),[6] 1395 and 1292 cm^{-1} (the C−OH stretching and bending vibration respectively), 1120 cm^{-1} (the C−O vibration), and 1045 cm^{-1} (C−O vibrations),[37] confirming the successful synthesis of PDA coating, which was beneficial in binding to U(VI). Regarding TNS-PDA/CNT, the additional bands at 458, 628, and 889 cm^{-1}, correspond to the crystal lattice vibration of [TiO_6] octahedron, vibrations of the Ti−O−Na bonds, and the Ti−O symmetric vibration of the nonbridging oxygen atoms, respectively, which corroborated the formation of $Na_2Ti_3O_7$.[38] For deep research into the surface chemical properties of the composites, the samples were characterized by XPS techniques (Figure 2d). Except C 1s (283.55 eV), the O 1s core photoionization signal (531.84 eV) was observed in CNT spectra, originating from contamination or/and surface defects.[39] In XPS spectra of TNS-PDA/CNT, however, the N

https://doi.org/10.1021/acsomega.4c05253
ACS Omega 2024, 9, 49108−49120

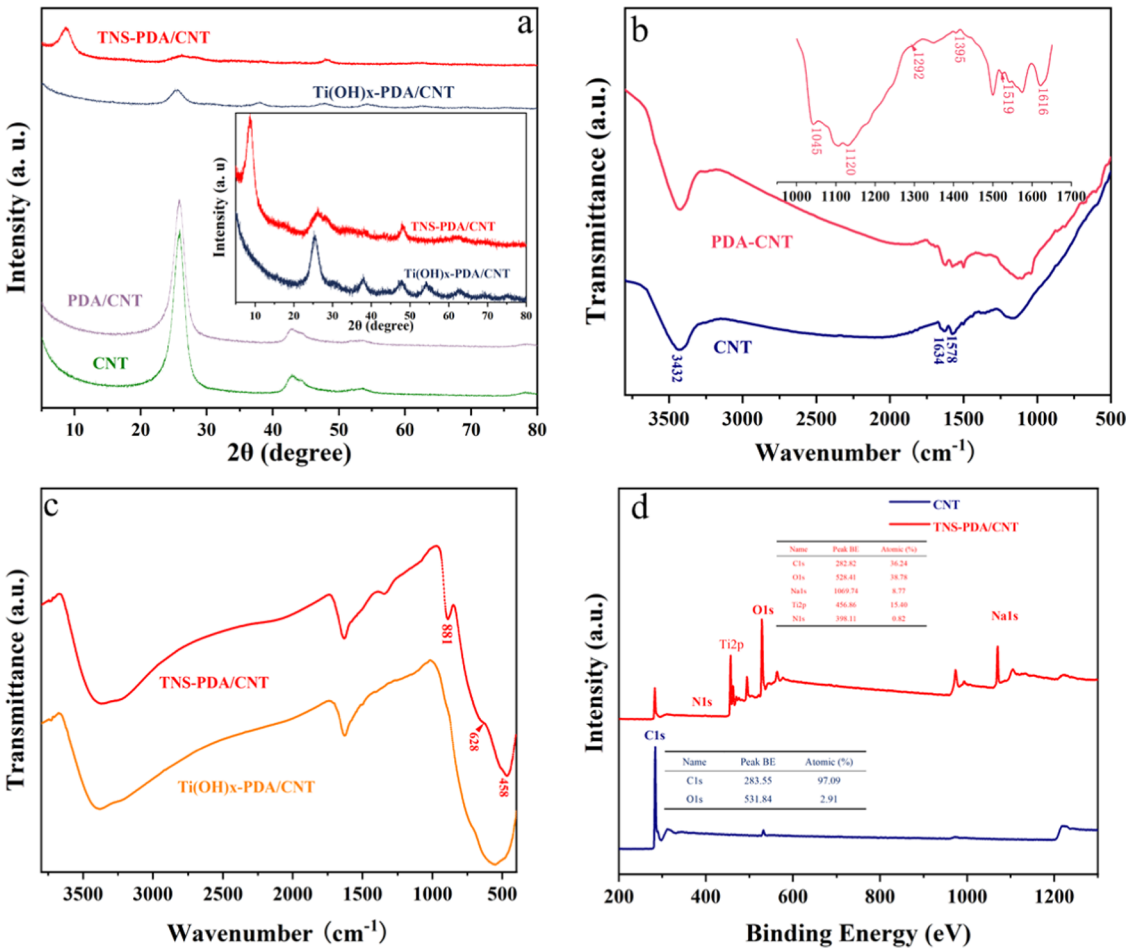

Figure 2. (a) XRD patterns of as-synthesized CNT, PDA/CNT, Ti(OH)$_x$-PDA/CNT, and TNS-PDA/CNT. The spectrum shown in the inset corresponds to Ti(OH)$_x$-PDA/CNT and TNS-PDA/CNT. (b) FT-IR spectra of pure CNT and PDA/CNT. (c) FTIR spectra of Ti(OH)$_x$-PDA/CNT and TNS-PDA/CNT. (d) XPS spectra of CNT and TNS-PDA/CNT.

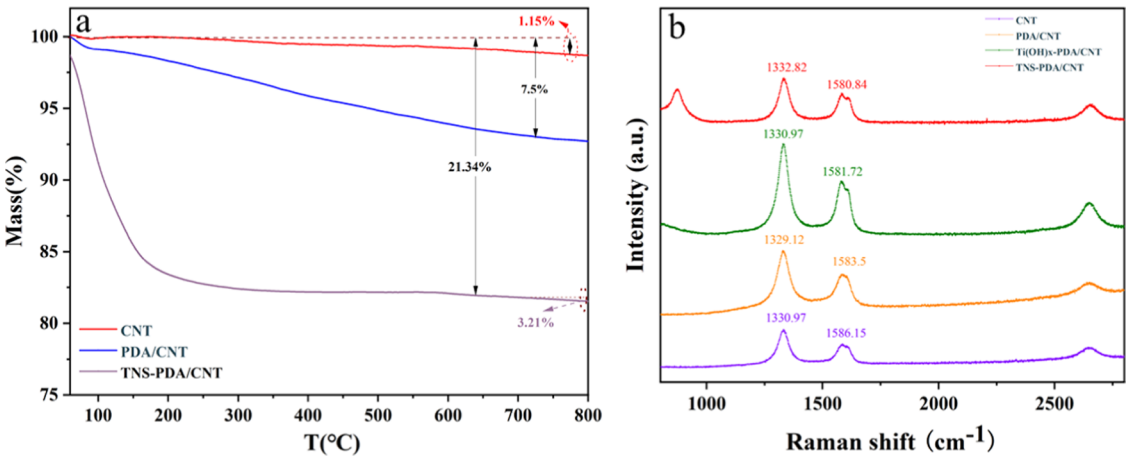

Figure 3. (a) Thermogravimetric curves of pure CNT, PDA/CNT, and TNS-PDA/CNT composites. (b) Raman spectra of CNT, PDA/CNT, Ti(OH)$_x$-PDA/CNT, and TNS-PDA/CNT.

1s peak at 398 eV came from the PDA catalysis, while the peaks at 1069.74 eV (Na 1s) and 456.86 eV (Ti 2p) revealed the presence of TNS. The above analysis coincided with the results of XRD and FTIR, which confirmed the materials were successfully prepared.

TGA could provide more information about the modification of CNT with PDA and TNS. As shown in Figure 3a, a weight loss of 1.81% for pristine CNT was observed, corresponding to physically adsorbed water, which implied that the CNT was thermally stable and had a lack of functional groups. For PDA/CNT and TNS-PDA/CNT, however, the TGA profiles illustrated a weight loss of 7.92 and 21.59%, respectively. Moreover, at temperatures above 730 °C, there was a 3.21% weight loss for TNS-PDA/CNT, which was

https://doi.org/10.1021/acsomega.4c05253
ACS Omega 2024, 9, 49108−49120

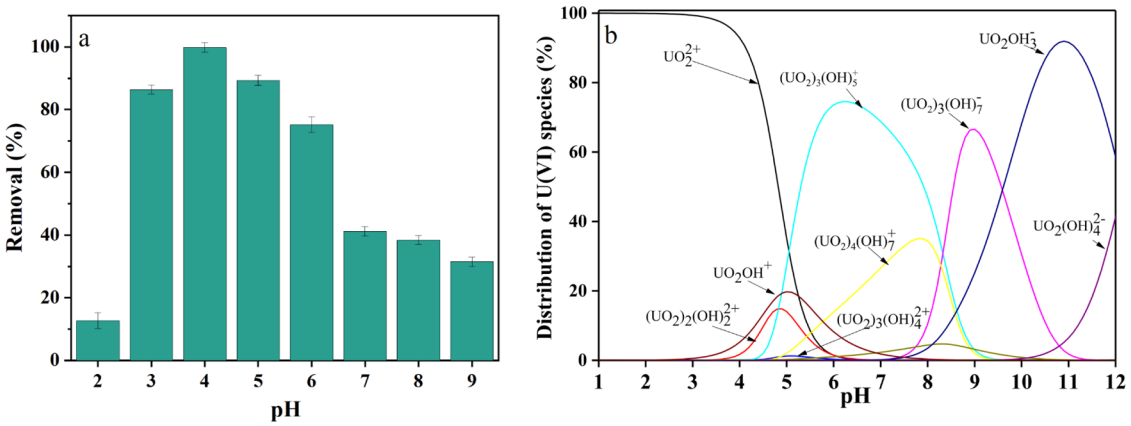

Figure 4. (a) Effect of pH on the U(VI) adsorption capacity. (b) Relative proportion of U(VI) species as a function of solution pH (initial U(VI) =20 mg/L, adsorbent dose = 0.2 g/L, temperature = 298 K).

probably related to the phase transformation.[40] The significant difference in the TGA profiles reflected the successful attachment of PDA and TNS to the CNT surface.[41,42]

Raman spectroscopy is a useful tool for studying the structural characteristics of the samples (Figure 3b). For CNT, two distinct Raman channels appeared at about 1330 and 1586 cm^{-1}, respectively. The first characteristic peak at 1330 cm^{-1}, known as the D band, corresponded to the characteristics of disorder in the carbon system resulting from the defect of carbon nanotube ends and bent sheets, and another characteristic peak at 1586 cm^{-1} (G band) reflected the in-plane mode of sp^2 carbon atoms of the graphite structure. After modifications, the G band had a slight shift from 1586 to 1583 cm^{-1} for PDA/CNT and 1580 cm^{-1} for TNS-PDA/CNT, respectively, which proved the successful modification of PDA and TNS. The ratio of the D band to G band intensity (I_D/I_G) was employed for assessing the degree of structural disorder. Compared with CNT (1.46), the I_D/I_G of CNT after modification was found to increase slightly, reflecting the formation of PDA and TNS on the surface of pure CNT. The unconspicuous difference of I_D/I_G values of CNT, PDA/CNTs, and TNS-PDA/CNT indicated that the structure of multiwalled carbon nanotubes remained basically unchanged.

3.2. Effect of pH. Solution pH can impact not only the U(VI) ion speciation and precipitation but also determine the surface properties of the adsorbents.[43,44] In Figure 4a, it could be observed that the adsorption capacity climbed up with the increase of pH at 2.0−5.0, reached the highest U(VI) adsorption capacity at pH 5.0, and subsequently declined when pH continued to increase. Such behavior could be explained by analyzing the U(VI) species distribution at different pH values. Figure 4b displayed the relative proportion of U(VI) species as a function of solution pH, as determined by Visual MINTEQ.[45] As the solution pH increased, there was an accumulation of negatively charged U(VI) species and a reduction in positively charged ones. At pH < 5, UO_2^{2+} was the major species in solution. When pH = 5−8, multiple uranium-hydroxide species, such as $(UO_2)_2(OH)_2^{2+}$, UO_2OH^+, $(UO_2)_3(OH)_4^{2+}$, $(UO_2)_4(OH)_7^+$, and $(UO_2)_3(OH)_5^+$, appeared in solution. However, the negatively charged species of $UO_2(OH)_3^-$ and $(UO_2)_3(OH)_7^-$ were found to be the dominating species as the solution pH exceeded 8.0.

The modes of interaction of U(VI) with TNS-PDA/CNT at different pH values could be described by the following reactions:

(1) At pH < 5, the dominant species is UO_2^{2+}, thus the important modes of action are as follows

$$UO_2^{2+} + 2NaO \equiv Ti_3O_7 \rightarrow (UO_2)O_2 \equiv Ti_3O_7 + 2Na^+ \quad (4)$$

(2) In the pH range of 4−8, multiple uranium-hydroxide species ($(UO_2)_2(OH)_2^{2+}$, UO_2OH^+, $(UO_2)_3(OH)_4^{2+}$, $(UO_2)_4(OH)_7^+$, and $(UO_2)_3(OH)_5^+$) become an important existing form and possible modes of action were expressed by eqs 5−9.

$$UO_2(OH)^+ + NaO \equiv Ti_3O_7 \rightarrow UO_2(OH)O \equiv Ti_3O_7 + Na^+ \quad (5)$$

$$(UO_2)_2(OH)_2^{2+} + 2NaO \equiv Ti_3O_7 \rightarrow (UO_2)_2(OH)_2O_2 \equiv Ti_3O_7 + 2Na^+ \quad (6)$$

$$(UO_2)_3(OH)_5^+ + NaO \equiv Ti_3O_7 \rightarrow (UO_2)_3(OH)_5O \equiv Ti_3O_7 + Na^+ \quad (7)$$

$$(UO_2)_3(OH)_4^{2+} + 2NaO \equiv Ti_3O_7 \rightarrow (UO_2)_3(OH)_4O_2 \equiv Ti_3O_7 + 2Na^+ \quad (8)$$

$$(UO_2)_4(OH)_7^+ + NaO \equiv Ti_3O_7 \rightarrow (UO_2)_4(OH)_7O \equiv Ti_3O_7 + Na^+ \quad (9)$$

(3) At pH > 8, in the negatively charged species of $UO_2(OH)_3^-$ and $(UO_2)_3(OH)_7^-$, electrostatic repulsion makes ion exchange impossible, and the nitrogen and oxygen functional groups of PDA layer play a certain role in the adsorption process. The surface complexation can be summarized as follows

$$H_2Y^2 + UO_2^{2+} = UO_2Y^{2-} + 2H^+ \quad (10)$$

where H_2Y_2 represents the PDA molecules.

3.3. Effect of Adsorbent Dose. To compare the adsorption capacity and the cost-effectiveness of CNT and

https://doi.org/10.1021/acsomega.4c05253
ACS Omega 2024, 9, 49108−49120

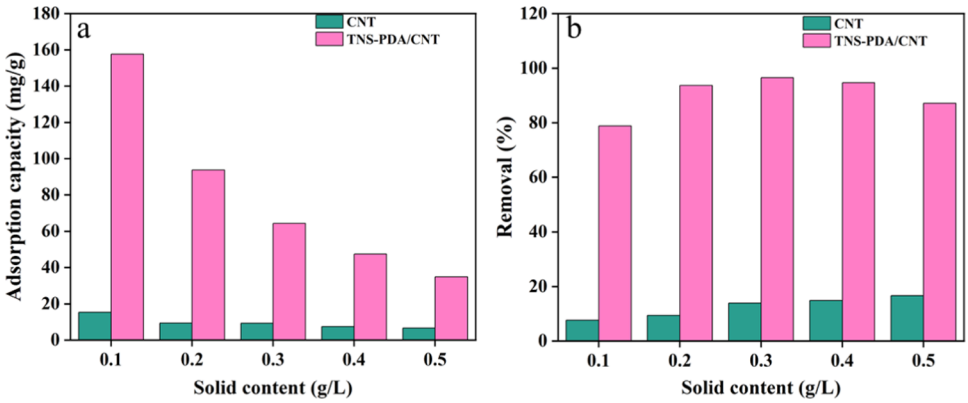

Figure 5. Effect of adsorbent dosage on U(VI): (a) adsorption capacity and (b) removal rate by CNT and TNS-PDA/CNT (initial U(VI)=20 mg/L, pH = 5.0, temperature = 298 K).

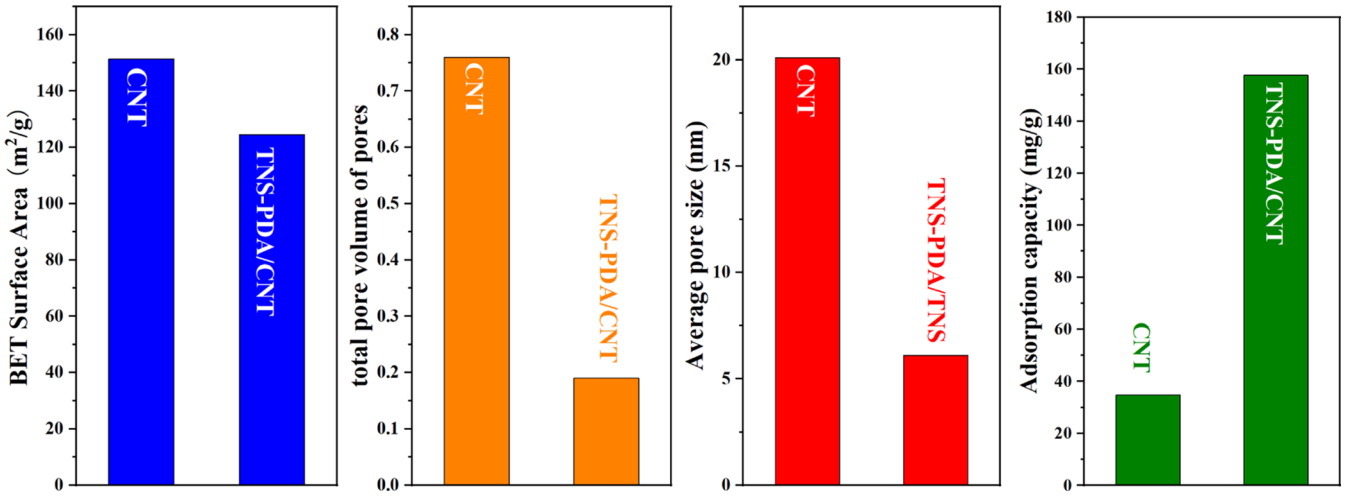

Figure 6. Balanced adsorption capacity of removing U(VI), intuitive comparison of surface areas, pore volume, and BJH average pore diameter of synthesized samples (initial U(VI)=20 mg/L, adsorbent dose = 0.2 g/L, pH = 5.0, temperature = 25 °C).

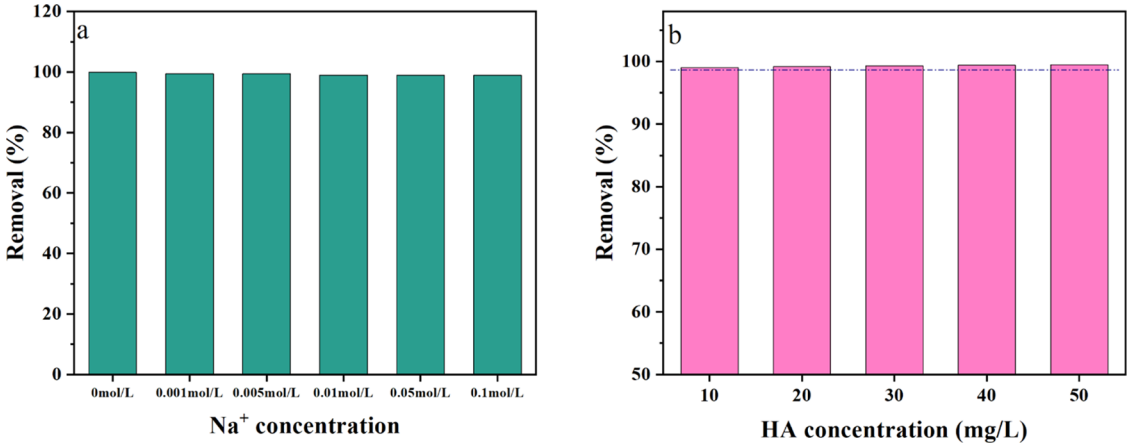

Figure 7. Effect of (a) ionic strength and (b) HA on U(VI) adsorption by TNS-PDA/CNT (initial U(VI)=20 mg/L, adsorbent dose = 0.2 g/L, pH = 5.0, temperature = 298 K).

TNS-PDA/CNT, we investigate the effect of adsorbent dose on the U(VI) uptake amount at V = 20 mL, C_0 = 50 mg/L, t = 60 min, and T = 298 K. In Figure 5, we could clearly observe that the increase in adsorbent from 0.005 to 0.025 g led to a decrease of the adsorption capacity from 157.67 to 34.84 mg/g for TNS-PDA/CNT and from 15.25 to 6.65 mg/g for CNT, respectively. This tendency was as expected because of the fact that the distribution coefficient (K_d) decreased with the increasing amount of adsorbent due to the solid effect.[46,47] However, the removal rate of U(VI) on two adsorbents first increased with adsorbent concentration from 0.1 to 0.3 g/L because of the existence of additional available active sites, and a further increase in the amount of adsorbent did not have a significant improvement in removal rate because the remaining

https://doi.org/10.1021/acsomega.4c05253
ACS Omega 2024, 9, 49108−49120

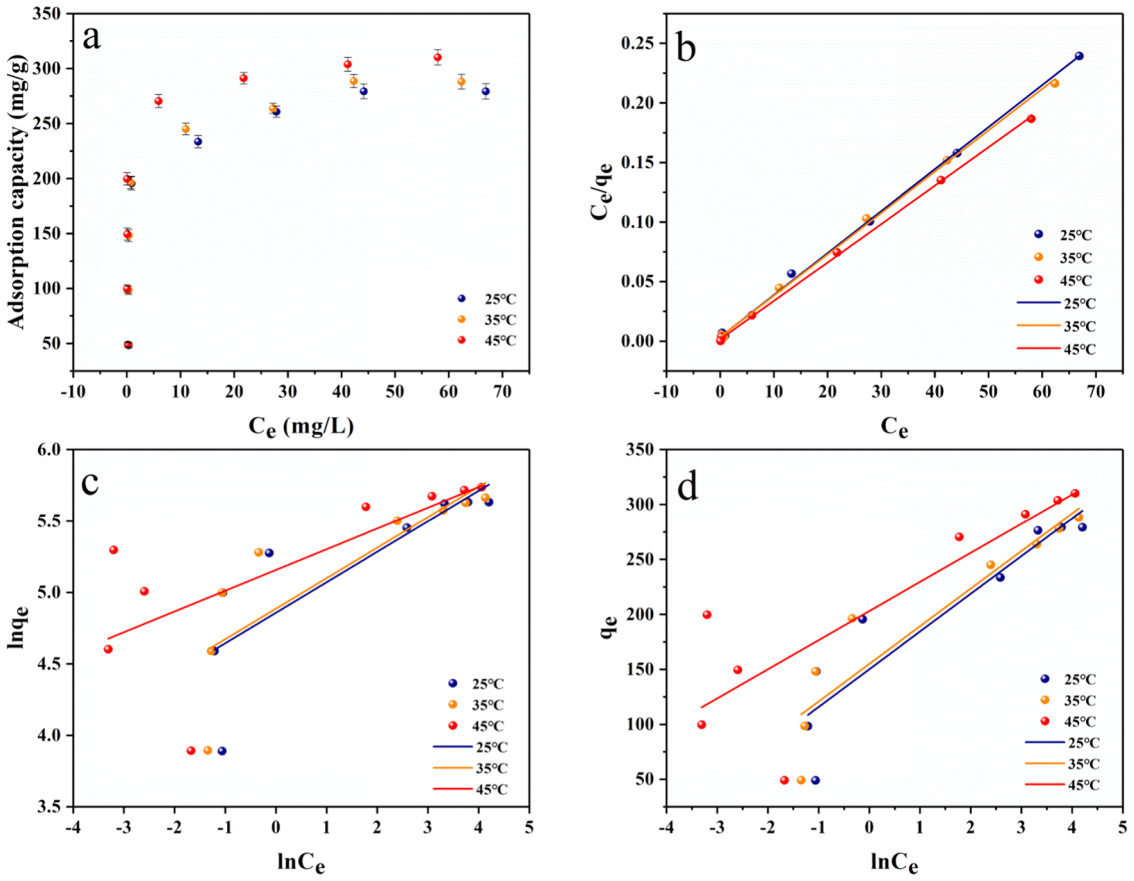

Figure 8. (a) Adsorption isotherm of TNS-PDA/CNT for U(VI) at different temperatures. Linear plots of (b) Langmuir, (c) Freundlich, and (d) Temkin isotherm models for U(VI) uptake by CNT and TNS-PDA/CNT.

U(VI) ions in solution are less (since all U(VI) ions were completely removed (100%) using 0.3 g/L).[48,49] Moreover, the adsorption amount of U(VI) by TNS-PDA/CNT (157.67 mg/g) was much higher than that of U(VI) by CNT(15.25 mg/g). This implied that (1) the participation of PDA created binding sites (catechol and amine groups) for U(VI) adsorption; (2) the introduction of TNSs supplied more ion exchange sites (Na^+) for interacting with U(VI). In summary, the synergistic interaction of CNT, PDA, and TNS was conducive to a much enhanced adsorption capacity as compared with the counterparts. Figure 6 reveals the relationship between the specific surface area (or pore volume) and adsorption capacity. It could be seen that the decrease of the specific surface area (or pore volume) of TNS-PDA/CNT, as compared to that of CNT, did not lead to a decrease of adsorption capacity, but led to a significant increase, which confirmed that the PDA coating and TNS provided abundant groups to compensate for the loss of adsorption capacity caused by the specific surface area.

3.4. Effect of Ionic Strength and Humic Acid Concentration. The adsorption performance of U(VI) by TNS-PDA/CNT as a function of ionic strength was investigated by launching experiments ranging from 0 to 0.1 mol/L NaCl solution. As plotted in Figure 7a, the removal rate of U(VI) on TNS-PDA/CNT slightly declined with the increase of NaCl concentration because (1) high ionic strength resulted in aggregation of TNS-PDA/CNT by altering electrostatic interaction, and thus inhibiting adsorption;[50] (2) high ionic strength intensified the competition of adsorption sites between U(VI) and Na^+ due to screening effect;[51] (3) high ionic strength altered the activity coefficient of U(VI), and thus restrained U(VI) transfer from the solution to adsorbent surfaces.[52] However, no significant variation was observed with NaCl concentration increasing, which revealed a sign of inner-sphere surface complexation, indicating the formation of chemical bonds between U(VI) and the surface functional groups.[53] Humic acid is a kind of macromolecular organic matter widely existing in natural water, which plays a significant role in the migration and transformation of heavy metal in the waterbody. Therefore, the influence of humic acid (HA) on adsorption capacity and removal rate was investigated and illustrated in Figure 7b, respectively. HA had a slight promoting effect on the U(VI) adsorption with an increase of 0.5% from 0 to 50 mg/L. The results were in line with Song et al.'s findings.[54] The positive effect could be explained by changing surface properties (surface charge and functional groups) of the adsorbent surface due to the presence of HA.[55]

3.5. Adsorption Kinetics. The U(VI) immobilization performance of TNS-PDA/CNT was explored at 25 °C from 2 to 80 min, and the results are illustrated in Figure S4. With the extension of contact time, the adsorbed amount of U(VI) onto TNS-PDA/CNT increased dramatically and gradually achieved adsorption saturation (see Supporting Information Figure S4). However, the U(VI) uptake on TNS-PDA/CNT fulfilled equilibrium at less than 20 min.

To clarify the kinetic mechanism, pseudo-first-order eq (S1) and pseudo-second-order eq (S2) were applied to simulate the kinetic data, respectively. The corresponding parameters are

https://doi.org/10.1021/acsomega.4c05253
ACS Omega 2024, 9, 49108−49120

tabulated in Table S1. As can be clearly seen in Table S1, the pseudo-second-order model was more suitable to describe the adsorption process according to the higher correlation coefficients (R^2 = 0.992 for TNS-PDA/CNT) (see Supporting Information Table S1). In addition, a good agreement between experimental values and calculated values derived from pseudo-second-order also suggested that the rate-controlling step was chemical adsorption through sharing or exchanging of electrons between U(VI) and adsorbents.[56]

To further investigate the possibility of intraparticle diffusion, the intraparticle diffusion kinetic models were also used to describe the kinetic process, and it was expressed as eq 11[57]

$$q_t = k_{di} t^{0.5} + C \tag{11}$$

where k_{di} (mg/(g·min$^{0.5}$)) is the intraparticle diffusion rate constant of stage i, t (min) is the contact time, and C_i (mg/g) is the constant proportional to the extent of boundary layer thickness. The values of k_{di} and C could be calculated from the slope and intercept of the linear of qt against $t^{0.5}$ and are summarized in Table S1. In general, typically, the adsorption process is governed by intraparticle diffusion if the Weber–Morris plot (q_t vs $t^{1/2}$) aligns with a linear relationship with the kinetic data (see Supporting Information Table S1). However, if the fitting line of data points consists of two parts, two and more steps control the adsorption process.[58] From Figure S4d, we could obviously find that the entire adsorption process was composed of two linear plots (see Supporting Information Figure S4). The initial sharper portion stood for instantaneous adsorption, corresponding to the diffusion of adsorbates from the solution phase to the adsorbent surface or boundary layer diffusion of solute molecules. The second linear portion gradually reached equilibrium with the decrease of available active sites, corresponding to a coordination reaction between U(VI) and active sites.[30]

3.6. Adsorption Isotherm Studies. To obtain more information about the distribution of U(VI) between the adsorbent surface (milligrams per gram) and the solution phase (mg/L), we measured the adsorption isotherm (Figure 8). With the initial concentration increasing, the adsorption capacity first increased and then progressively reached adsorption saturation (310.28 mg/g at 45 °C). The tendency toward U(VI) adsorption was a result of the driving force generated by the concentration gradient.[59] For interpretation of the isotherm data, the Langmuir, Freundlich, and Tempkin isotherm models were used to describe the equilibrium data.[48,60,61] The fitting plot of three models is illustrated in Figure 8b–d, and the calculated parameters by eqs (S3–S5) are summarized in Table 1. By comparing the correlation coefficient of different models, the Langmuir model was more suitable to describe adsorption data in three models, suggesting the monolayer adsorption of U(VI) onto uniform surface with energetically identical sites. Meanwhile, the theoretical maximum adsorption capacity of CNTs@PDA@TNSs was 309.60 mg/g at 45 °C, which was much higher than that of other advanced adsorbents listed in Table 2, such as carbonaceous nanofibers,[8] 4-aminothiophenol-functionalized graphene oxide composite,[62] phosphate-functionalized graphene oxide,[53] multishelled Fe_3O_4@MnO_x,[54] niobate/titanate nanoflakes,[33] sodium titanate nanospheres,[63] amidoxime-functionalized chitosan beads,[64] AO-*g*-MWCNTs,[65] and polydopamine/graphene oxide.[22] Therefore, it could be concluded that CNTs@PDA@TNS was an excellent adsorbent to meet the requirements of eliminating metal ions from wastewater.

Table 1. Parameters of Langmuir, Freundlich, and Tempkin Models of U(VI) Adsorption on TNS-PDA/CNT

		TNS-PDA/CNT		
equations	parameters	25 °C	35 °C	45 °C
Langmuir model	Q_{max} (mg/g)	283.27	288.18	309.60
	K_L (L/mg)	0.9778	0.9612	1.9
	R^2	0.999	0.999	0.999
Freundlich model	K_F (mg$^{(1-n)}$L^n/g)	128.858	132.587	173.797
	n	4.6863	4.6867	6.8842
	R^2	0.817	0.829	0.712
Tempkin	α (L/mg)	80.22	93.54	2158.25
	b_T (kJ/mol)	72.28	74.89	99.89
	R^2	0.849	0.863	0.724

Table 2. Comparison of the U(VI) Adsorption Capacity in the Literature

adsorbents	experimental conditions	adsorption behavious	q_{max} (mg/g)	refs
carbonaceous nanofibers	pH = 4.5, T = 298 K	Langmuir isotherm	125	8
4-aminothiophenol-functionalized graphene oxide composite	pH = 5.5, T = 298 K	Langmuir model	281.69	26
phosphate-functionalized graphene oxide	pH = 4.0, T = 303 K	Langmuir model	251.7	53
multishelled Fe_3O_4@MnO_x	pH = 5.0, T = 298 K	Langmuir model	106.72	54
niobate/titanate nanoflakes	pH = 5.0	Langmuir model	298.5	33
amidoxime-functionalized chitosan beads	pH = 6.0, T = 298 K	Langmuir model	117.65	64
AO-*g*-MWCNTs	pH = 4.5, T = 298 K	Langmuir model	145	65
polydopamine/graphene oxide	pH = 4.0, T = 293 K	Langmuir model	145.39	22
CNTs@PDA@TNSs	pH = 4.0, T = 298 K	Langmuir model	283.286	in this study

The dimension parameter R_L can reflect the essential characteristic of the Langmuir isotherm and is expressed by eq 12

$$R_L = \frac{1}{1 + bC_0} \tag{12}$$

where C_0 (mg/L) is the initial concentration of U(VI) and b (L/mg) is the Langmuir constant. The dimension parameter R_L ranged from 0 to 1, which suggested that the U(VI) adsorption by TNS-PDA/CNT could be identified as favorable.[66] Moreover, the R_L value was close to zero with increasing U(VI) initial concentration, suggesting that a high initial concentration was beneficial for the irreversible adsorption of U(VI) on TNS-PDA/CNT.

3.7. Thermodynamic Study. To obtain additional information about the inherent energy change and adsorption mechanism, thermodynamic parameters, i.e., standard entropy $\Delta S°$ (J/(mol·K)), standard enthalpy $\Delta H°$ (kJ/mol), and standard free energy $\Delta G°$ (kJ/mol) for U(VI) elimination

https://doi.org/10.1021/acsomega.4c05253
ACS Omega 2024, 9, 49108−49120

process, were calculated by eqs 13 and 14, and the results are summarized in Table 3.

$$\ln K_d = -\frac{\Delta H^\circ}{RT} + \frac{\Delta S^\circ}{R} \quad (13)$$

$$\Delta G^\circ = -RT \ln K_d \quad (14)$$

Table 3. Thermodynamic Parameters of U(VI) Adsorption on TNS-PDA/CNT at 298, 308, and 318 K

	T (K)	ΔH° (kJ/mol)	ΔS° (J/(mol·K))	ΔG° (kJ/mol)
TNS-PDA/CNT	298	15.44	87.98	−10.808
	308			−11.603
	318			−12.572

Specifically, the ΔH° value was positive (15.44 kJ/mol), indicating that the adsorption was endothermic, which could be illuminated by the following reasons: (1) Higher temperature promoted the diffusion and migration of U(VI) through the external boundary layer and internal pores of the adsorbents.[67] (2) U(VI) coordinated water needed to be dehydrated for the complexation with surface sites of TNS-PDA/CNT prior to adsorption. This process was endothermic and more favorable at higher temperatures.[68] (3) The increasing temperature was propitious to the availability of more active sites.[69] The positive value of ΔS° (87.98 J/(mol·K)) indicated the enhanced disorderliness at the solid−water interfaces after adsorption.[70] The ΔG° value was negative (−10.808 kJ/mol) and shifted to a high negative value (−12.572 kJ/mol) with the increase of temperature from 25 to 45 °C, and the high temperature was helpful to remove U(VI).[71]

3.8. Adsorption Mechanisms. To investigate the adsorption mechanisms from the perspective of spectral analysis, TNS-PDA/CNT materials before and after adsorption were characterized by the XRD, FTIR, and XPS techniques. Figure 9a exhibits the XRD patterns of TNS-PDA/CNT and U-TNS-PDA/CNT. Apparently, the first peaks, corresponding to the interlayer distance of TNSs, showed a slight change from 8.69 to 8.33°, which reflected the stretching of the interlayer structure due to the substitution of Na^+/H^+ ions by the U(VI) ions.[71] Simultaneously, other characteristic peaks did not change significantly, suggesting there was no distinct damage to TNS-PDA/CNT during the U(VI) adsorption process.[72,73] Moreover, in the FTIR spectra of U-TNS-PDA/CNT (Figure 9b), a new characteristic adsorption band (representing O═U═O antisymmetric vibration) emerged at round 910 cm^{-1}, which has a significant red shift relative to the aqueous UO_2^{2+} species (960 cm^{-1}), suggesting the binding interaction between U(VI) and the surface functional group of material.[74,75] The disappearance of the Ti−O−Na peak at 628 cm^{-1} suggested that ion exchange has a certain contribution to the adsorption process,[49] which further confirmed the results of XRD.

To further verify the potential of the interaction mechanism between U(VI) and TNS-PDA/CNT, XPS results of the adsorbent before and after adsorption of U(VI) are presented in Figure 10. Compared with CNTs@PDA@TNSs, the TNS-PDA/CNT after the capture of U(VI) showed a new peak of U 4f, while the intensity of the Na 1s peak (1070.2 eV) became weaker, which confirmed that ion exchange reaction participated in sequestering U(VI) (Figure 10a,b). The core-level N 1s spectrum of the TNS-PDA/CNT could be fitted into three characteristic peaks at binding energy 397.90 (═N−), 398.89 (−NH−), and 401.38 eV ($-NH_2$), respectively (Figure 10c). However, except for the ═N− peak, the other two peaks shifted to the higher binding energy after adsorption (Figure 10d). Similarly, in the high-resolution O 1s spectrum, the peaks at 528.41 eV migrated to a higher binding energy of 528.76 eV (Figure 10e). The shift to higher binding energy implied the occurrence of the complex reaction, in which a long pair of electrons in the O/N atom (electron donor) could be provided to uranium atom (electron acceptors), resulting in the reduction of electron cloud density around the O/N atom.[38,76] From the high-resolution U 4f spectrum, U $4f_{7/2}$ and U $4f_{5/2}$ located at 382.08 and 393.08 eV were observed (see Supporting Information Figure S5).

In Figure 10f, Ti 2p peaks center at 462.82 and 457 eV with 5.82 eV spin-energy separation were assigned to the spin−orbit splitting of the Ti 2p components.[71] After binding with U(VI), the two peaks had a slight change, and the spin energy remained the same, indicating the stability of the skeleton trititanate structure in the adsorption process. Based on the above results, we tentatively proposed the possible adsorption mechanism of U(VI) and TNS-PDA/CNT involved ion exchange interaction between U(VI) and the interlayered Na^+ ions as well as surface complexation from the plentiful

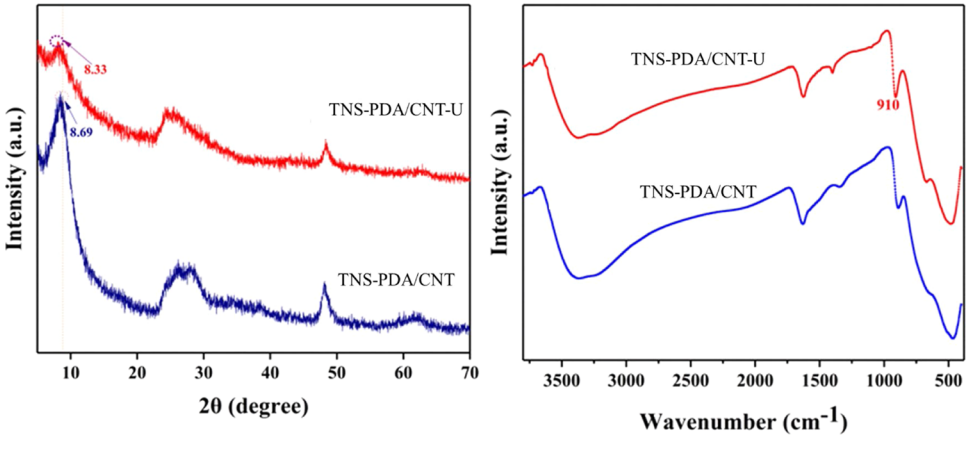

Figure 9. XRD patterns (a) and FTIR spectra (b) of TNS-PDA/CNT before and after the adsorption of U(VI).

https://doi.org/10.1021/acsomega.4c05253
ACS Omega 2024, 9, 49108−49120

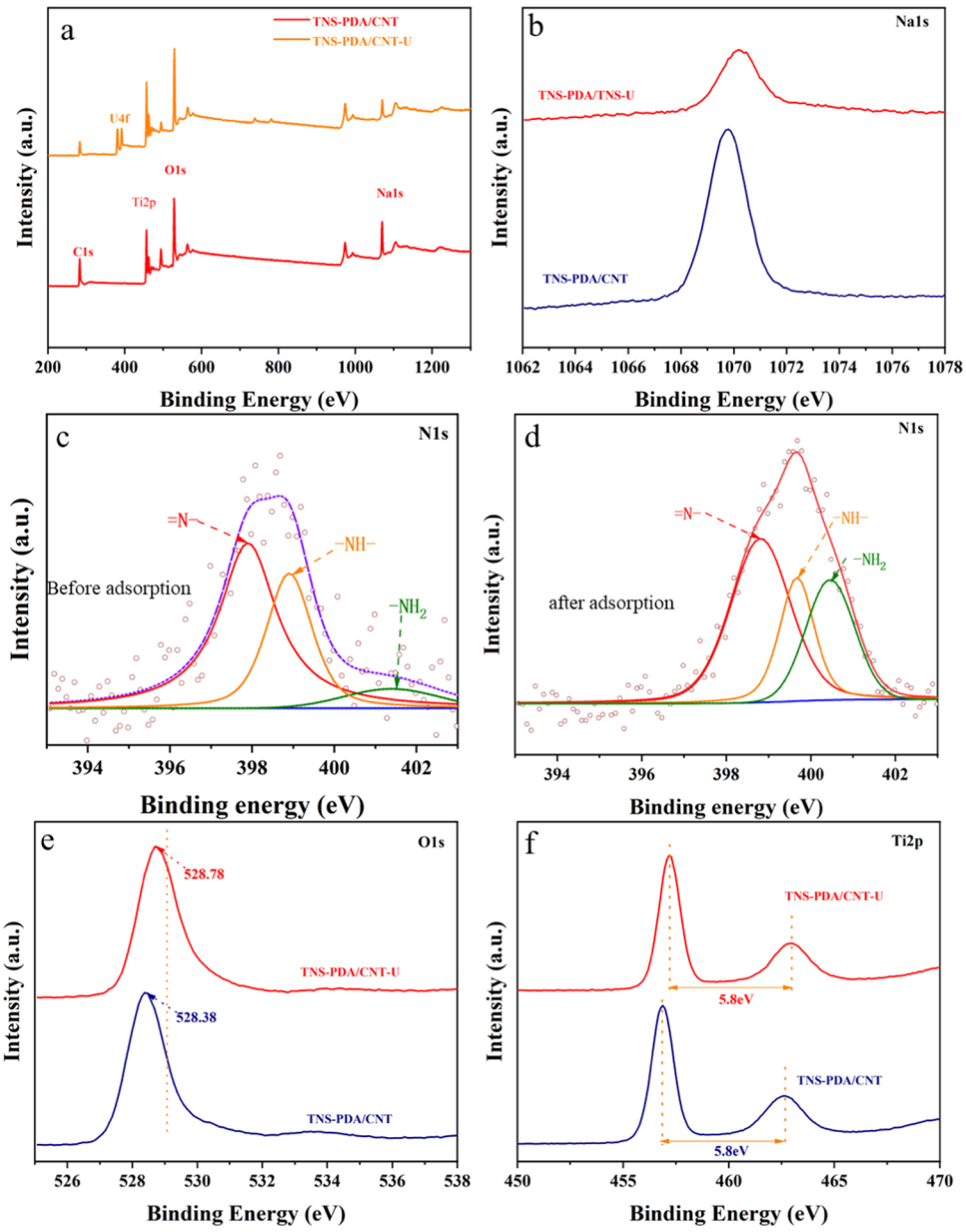

Figure 10. XPS spectra of (a) TNS-PDA/CNT and U-TNS-PDA/CNT. High-resolution XPS spectra of (b) Na 1s, (c and d) N 1s, (e) O 1s, and (f) Ti 2p.

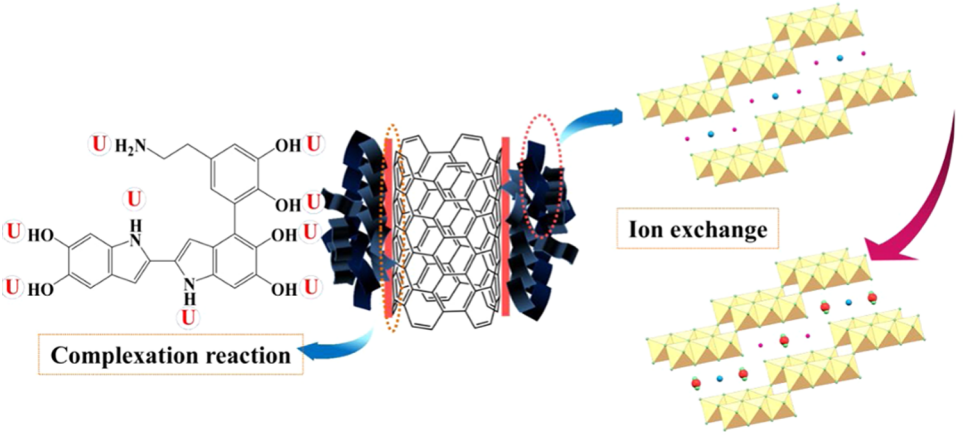

Figure 11. Conceptualized representation of the adsorption of U(VI) by TNS-PDA/CNT.

https://doi.org/10.1021/acsomega.4c05253
ACS Omega 2024, 9, 49108−49120

catechol and amine functional groups, as illustrated in Figure 11.

4. CONCLUSIONS

TNS-PDA/CNT was fabricated by in situ growth of titanate sheets onto a polydopamine-encapsulated CNT surface. The as-synthesized adsorbent exhibited outstanding adsorption capacity, which was approximately 10 times that of pure CNTs. The optimum pH value was found to be 4.0, and the U(VI) adsorption by CNTs@PDA@TNSs was slightly inhibited by ionic strength. The good fitting of the adsorption process to the pseudo-second-order kinetics indicated the nature of the chemical. The Langmuir model was more suitable for describing U(VI) adsorption by CNTs@PDA@TNSs, implying the monolayer adsorption with a maximum adsorption capacity of 309.60 mg/g at pH 5.0 and temperature = 45 °C. The thermodynamic study confirmed that the adsorption process was spontaneous and endothermic. The analysis of XRD, FTIR, and XPS revealed the essence of adsorption involved ion exchange between U(VI) and the interlayered Na^+ ions as well as surface complexation from the plentiful catechol and amine functional groups. All findings indicated that TNS-PDA/CNT had enormous potential for capturing U(VI) from high salinity and the polyion coexisting system.

■ ASSOCIATED CONTENT

Supporting Information

The Supporting Information is available free of charge at https://pubs.acs.org/doi/10.1021/acsomega.4c05253.

Adsorption kinetics and isotherm models; SEM image and elemental mapping of TNS-PDA/CNT and TNS-PDA/CNT-U; and adsorption kinetic curves and parameters for U(VI) (PDF)

■ AUTHOR INFORMATION

Corresponding Author

Yuzhi Zhou − *School of Earth and Environment, Anhui University of Science and Technology, Huainan 232001, P. R. China; Anhui Province Engineering Laboratory of Water and Soil Resources Comprehensive Utilization and Ecological Protection in High Groundwater Mining Area, Huainan 232001, P. R. China;* orcid.org/0009-0004-3693-5622; Email: zhouyuzhi1218@126.com

Authors

Zhiyang Jiang − *School of Earth and Environment, Anhui University of Science and Technology, Huainan 232001, P. R. China*

Wenshuo Wang − *School of Earth and Environment, Anhui University of Science and Technology, Huainan 232001, P. R. China*

Zheng Yin − *School of Chemistry and Chemical Engineering, South China University of Technology, Guangzhou 510641, P. R. China*

Mingze Zhao − *School of Earth and Environment, Anhui University of Science and Technology, Huainan 232001, P. R. China*

Lei Yu − *School of Earth and Environment, Anhui University of Science and Technology, Huainan 232001, P. R. China*

Sijie Ren − *School of Earth and Environment, Anhui University of Science and Technology, Huainan 232001, P. R. China*

Han Xiao − *School of Earth and Environment, Anhui University of Science and Technology, Huainan 232001, P. R. China*

Yanfang Ma − *School of Earth and Environment, Anhui University of Science and Technology, Huainan 232001, P. R. China*

Complete contact information is available at: https://pubs.acs.org/10.1021/acsomega.4c05253

Author Contributions

Z.J.: investigation, software, data curation, validation, writing—original draft, writing—review and editing. Y.Z.: resources, validation, funding acquisition, investigation, project administration. W.W.: resources, validation, writing—review and editing, data curation. Z.Y.: software, data curation, writing—original draft, writing—review and editing. M.Z. and L.Y.: investigation, validation, writing—original draft. S.R., H.X., and Y.M.: investigation, data curation, writing—review and editing.

Notes

The authors declare no competing financial interest.

■ ACKNOWLEDGMENTS

The authors are grateful to the financial support provided by Natural Science Research Project of Anhui Educational Committee (No. 2023AH051177), Scientific Research Foundation for High-level Talents of Anhui University of Science and Technology (No. 2022yjrc13), the Opening Foundation of Anhui Province Engineering Laboratory of Water and Soil Resources Comprehensive Utilization and Ecological Protection in High Groundwater Mining Area (No.:2022-WSREP-MA-05), and the Opening Foundation of Anhui Province Engineering Laboratory for Mine Ecological Remediation (No. KS-2022-002). Related characterization analysis has been supported by Shiyanjia Lab (www.shiyanjia.com). The authors express their sincere thanks and gratitude to the anonymous reviewers for their positive comments and constructive suggestions.

■ REFERENCES

(1) Zhang, X.; Yang, X.; Rong, Q.; Liu, X.; Zhou, Y.; Yang, H.; Wang, G.; Chen, Z.; Wang, X. Enrichment and separation of radionuclides by organic polymer materials: a review. *ACS ES&T Eng.* **2024**, *4* (2), 250−268.

(2) Jalbani, N.; Soylak, M. Spectrophotometric determination of uranium using chromotrope 2R complexes. *J. Radioanal. Nucl. Chem.* **2014**, *301*, 263−268.

(3) Mellah, A.; Chegrouche, S.; Barkat, M. The precipitation of ammonium uranyl carbonate (AUC): thermodynamic and kinetic investigations. *Hydrometallurgy* **2007**, *85* (2−4), 163−171.

(4) Rana, D.; Matsuura, T.; Kassim, M. A.; Ismail, A. F. Radioactive decontamination of water by membrane processes - A review. *Desalination* **2013**, *321*, 77−92.

(5) Rokop, D. J.; Perrin, R. E.; Knobeloch, G. W.; Armijo, V. M.; Shields, W. R. Thermal Ionization Mass Spectrometry of Uranium with Electrodeposition as a Loading Technique. *Anal. Chem.* **1982**, *54* (6), 957−960.

(6) Meng, Q.; Wu, L.; Chen, T.; Xiong, Y.; Duan, T.; Wang, X. Constructing the Electron-Rich Microenvironment of an All-Polymer-Based S-Scheme Homostructure for Accelerating Uranium Capture from Nuclear Wastewater. *Environ. Sci. Technol.* **2024**, *58* (34), 15333−15342.

(7) Manos, M. J.; Ding, N.; Kanatzidis, M. G. Layered metal sulfides: exceptionally selective agents for radioactive strontium removal. *Proc. Natl. Acad. Sci. U.S.A.* **2008**, *105* (10), 3696−3699.
(8) Shah, F.; Soylak, M.; Kazi, T.; Afridi, H. Development of an extractive spectrophotometric method for uranium using MWCNTs as solid phase and arsenazo(III) as chromophore. *J. Radioanal. Nucl. Chem.* **2013**, *296*, 1239−1245.
(9) Hu, W.; Lu, S.; Song, W.; Chen, T.; Hayat, T.; Alsaedi, N. S.; Chen, C.; Liu, H. Competitive adsorption of U (VI) and Co (II) on montmorillonite: a batch and spectroscopic approach. *Appl. Clay Sci.* **2018**, *157*, 121−129.
(10) Iijima, S. Helical microtubules of graphitic carbon. *Nature* **1991**, *354*, 56−58.
(11) Gupta, V. K.; Agarwal, S.; Bharti, A. K.; Sadegh, H. Adsorption mechanism of functionalized multi-walled carbon nanotubes for advanced Cu (II) removal. *J. Mol. Liq.* **2017**, *230*, 667−673.
(12) Wang, Y.; Hu, L.; Zhang, G.; Yan, T.; Yan, L.; Wei, Q.; Du, B. Removal of Pb (II) and methylene blue from aqueous solution by magnetic hydroxyapatite-immobilized oxidized multi-walled carbon nanotubes. *J. Colloid Interface Sci.* **2017**, *494*, 380−388.
(13) Tan, L.; Liu, Q.; Jing, X.; Liu, J.; Song, D.; Hu, S.; Wang, J. Removal of uranium (VI) ions from aqueous solution by magnetic cobalt ferrite/multiwalled carbon nanotubes composites. *Chem. Eng. J.* **2015**, *273*, 307−315.
(14) Soylak, M.; Ozalp, O.; Uzcan, F. Magnetic nanomaterials for the removal, separation and preconcentration of organic and inorganic pollutants at trace levels and their practical applications: A review. *Trends Environ. Anal. Chem.* **2021**, *29*, No. e00109.
(15) Omidi, M. H.; Azad, F. N.; Ghaedi, M.; Asfaram, A.; Azqhandi, M. H. A.; Tayebi, L. Synthesis and characterization of Au-NPs supported on carbon nanotubes: Application for the ultrasound assisted removal of radioactive UO_2^{2+} ions following complexation with Arsenazo III: Spectrophotometric detection, optimization, isotherm and kinetic st. *J. Colloid Interface Sci.* **2017**, *504*, 68−77.
(16) Ren, X.; Chen, C.; Nagatsu, M.; Wang, X. Carbon nanotubes as adsorbents in environmental pollution management: A review. *Chem. Eng. J.* **2011**, *170* (2−3), 395−410.
(17) Zare, F.; Ghaedi, M.; Daneshfar, A.; Agarwal, S.; Tyagi, I.; Saleh, T. A.; Gupta, V. K. Efficient removal of radioactive uranium from solvent phase using AgOH−MWCNTs nanoparticles: Kinetic and thermodynamic study. *Chem. Eng. J.* **2015**, *273*, 296−306.
(18) Kończyk, J.; Żarska, S.; Ciesielski, W.; Kończyk, J.; Żarska, S.; Ciesielski, W. (2019). Adsorptive removal of Pb (II) ions from aqueous solutions by multi-walled carbon nanotubes functionalised by selenophosphoryl groups: Kinetic, mechanism, and thermodynamic studies. *Colloids Surf., A* **2019**, *75*, 271−282.
(19) Arica, T. A.; Kuman, M.; Gercel, O.; Ayas, E. Poly (dopamine) grafted bio-silica composite with tetraethylenepentamine ligands for enhanced adsorption of pollutants. *Chem. Eng. Res. Des.* **2019**, *141*, 317−327.
(20) Zhu, J.; Liu, Q.; Liu, J.; Chen, R.; Zhang, H.; Zhang, M.; et al. Investigation of uranium (VI) adsorption by poly (dopamine) functionalized waste paper derived carbon. *J. Taiwan Inst. Chem. Eng.* **2018**, *91*, 266−273.
(21) Li, X.; Lu, H.; Zhang, Y.; He, F.; Jing, L.; He, X. Fabrication of magnetic alginate beads with uniform dispersion of $CoFe_2O_4$ by the polydopamine surface functionalization for organic pollutants removal. *Appl. Surf. Sci.* **2016**, *389*, 567−577.
(22) Zhao, Z.; Li, J.; Wen, T.; Shen, C.; Wang, X.; Xu, A. Surface functionalization graphene oxide by polydopamine for high affinity of radionuclides. *Colloids Surf., A* **2015**, *482*, 258−266.
(23) Cho, J. H.; Shanmuganathan, K.; Ellison, C. J. Bioinspired catecholic copolymers for antifouling surface coatings. *ACS Appl. Mater. Interfaces* **2013**, *5* (9), 3794−3802.
(24) Wang, J.; Ma, J.; Zhang, C.; Li, X.; Song, S.; Wen, T.; et al. Fabrication of core−shell α-MnO_2@polydopamine nanocomposites for the efficient and ultra-fast removal of U(VI) from aqueous solution. *Dalton Trans.* **2019**, *48* (3), 971−981.
(25) Zhang, F.; Zhang, H.; Chen, R.; Liu, Q.; Liu, J.; Wang, C.; Sun, Z.; Wang, J. Mussel-inspired antifouling magnetic activated carbon for uranium recovery from simulated seawater. *J. Colloid Interface Sci.* **2019**, *534*, 172−182.
(26) Yang, H.; Ding, H.; Zhang, X.; Luo, X.; Zhang, Y. Immobilization of dopamine on Aspergillus niger microspheres (AM/PDA) and its effect on the U (VI) adsorption capacity in aqueous solutions. *Colloids Surf., A* **2019**, *583*, No. 123914.
(27) Kasuga, T.; Hiramatsu, M.; Hoson, A.; Sekino, T.; Niihara, K. Formation of Titanium Oxide Nanotube. *Langmuir* **1998**, *14* (12), 3160−3163.
(28) Kasuga, T.; Hiramatsu, M.; Hoson, A.; Sekino, T.; Niihara, K. Titania Nanotubes Prepared by Chemical Processing. *Adv. Mater.* **1999**, *11* (15), 1307−1311.
(29) Liu, W.; Zhao, X.; Wang, T.; Zhao, D.; Ni, J. Adsorption of U (VI) by multilayer titanate nanotubes: effects of inorganic cations, carbonate and natural organic matter. *Chem. Eng. J.* **2016**, *286*, 427−435.
(30) Zhu, J.; Liu, Q.; Liu, J.; Chen, R.; Zhang; Li, R.; H, R. Ni-Mn LDH-decorated 3D Fe-inserted and N-doped carbon framework composites for efficient uranium(VI) removal. *Environ. Sci.: Nano.* **2018**, *5* (2), 467−475.
(31) Zhao, M.; Wang, S.; Wang, H.; Qin, P.; Yang, D.; Sun, Y.; Kong, F. Application of sodium titanate nanofibers as constructed wetland fillers for efficient removal of heavy metal ions from wastewater. *Environ. Pollut.* **2019**, *248*, 938−946.
(32) Sheng, G.; Hu, J.; Alsaedi, A.; Shammakh, W.; Monaquel, S.; Ye, F.; Ahmad, B.; et al. Interaction of uranium (VI) with titanate nanotubes by macroscopic and spectroscopic investigation. *J. Mol. Liq.* **2015**, *212*, 563−568.
(33) Liu, X.; Du, P.; Pan, W.; Dang, C.; Qian, T.; Liu, H.; et al. Immobilization of uranium(VI) by niobate/titanate nanoflakes heterojunction through combined adsorption and solar-light-driven photocatalytic reduction. *Appl. Catal., B* **2018**, *231*, 11−22.
(34) Rajabi, M.; Mirza, B.; Mahanpoor, K.; Mirjalili, M.; Najafi, F.; Moradi, O.; Gupta, V. K.; et al. Adsorption of malachite green from aqueous solution by carboxylate group functionalized multi-walled carbon nanotubes: Determination of equilibrium and kinetics parameters. *J. Ind. Eng. Chem.* **2016**, *34*, 130−138.
(35) Yin, L.; Song, S.; Wang, X.; Niu, F.; Ma, R.; Yu, S.; et al. Rationally designed core-shell and yolk-shell magnetic titanate nanosheets for efficient U (VI) adsorption performance *. *Environ. Pollut.* **2018**, *238*, 725−738.
(36) Kathi, J.; Rhee, K. Y. Surface modification of multi-walled carbon nanotubes using 3-aminopropyltriethoxysilane. *J. Mater. Sci.* **2008**, *43*, 33−37.
(37) Zhang, Q.; Yang, Q.; Phanlavong, P.; Li, Y.; Wang, Z.; Jiao, T.; Peng, Q. Highly Efficient Lead(II) Sequestration Using Size-Controllable Polydopamine Microspheres with Superior Application Capability and Rapid Capture. *ACS Sustainable Chem. Eng.* **2017**, *5* (5), 4161−4170.
(38) Zhou, Y.; Li, Y.; Liu, D.; Wang, X.; Liu, D.; Xu, L. Synthesis of the inorganic-organic hybrid of two-dimensional polydopamine-functionalized titanate nanosheets and its efficient extraction of U(VI) from aqueous solution. *Colloids Surf., A* **2020**, *607*, No. 125422.
(39) Draouil, H.; Alvarez, L.; Causse, J.; Flaud, V.; Zaibi, M. A.; Bantignies, J. L.; Oueslati, M.; Cambedouzou, J. Copper hexacyanoferrate functionalized single-walled carbon nanotubes for selective cesium extraction. *New J. Chem.* **2017**, *41* (15), 7705−7713.
(40) Li, W.; Bai, Y.; Liu, C.; Yang, Z.; Feng, X.; Lu, X.; van der Laak, N. K.; Chan, K. Y. Highly thermal stable and highly crystalline anatase TiO_2 for photocatalysis. *Environ. Sci. Technol.* **2009**, *43* (14), 5423−5428.
(41) Meng, L.; Chan, Y.; Wang, H.; Dai, Y.; Wang, X.; Zou, J. Recycling of iron and silicon from drinking water treatment sludge for synthesis of magnetic iron oxide@SiO_2 composites. *Environ. Sci. Pollut. Res.* **2016**, *23*, 5122−5133.

https://doi.org/10.1021/acsomega.4c05253
ACS Omega 2024, 9, 49108−49120

(42) Wang, Y.; Liang, M.; Fang, J.; Fu, J.; Chen, X. Visible-light photo-Fenton oxidation of phenol with rGO-A-FeOOH supported on Al-doped mesoporous silica (MCM-41) at neutral pH: Performance and optimization of the catalyst. *Chemosphere* **2017**, *182*, 468−476.
(43) Deb, A. K. S.; Dwivedi, V.; Dasgupta, K.; Ali, S. M.; Shenoy, K. T. Novel amidoamine functionalized multi-walled carbon nanotubes for removal of mercury(II) ions from wastewater: Combined experimental and density functional theoretical approach. *Chem. Eng. J.* **2017**, *313*, 899−911.
(44) Alizadeh, B.; Ghorbani, M.; Salehi, M. A. Application of polyrhodanine modified multi-walled carbon nanotubes for high efficiency removal of Pb(II) from aqueous solution. *J. Mol. Liq.* **2016**, *220*, 142−149.
(45) Hyun, S. P.; Davis, J. A.; Sun, K.; Hayes, K. F. Uranium(VI) reduction by iron(II) monosulfide mackinawite. *Environ. Sci. Technol.* **2012**, *46* (6), 3369−3376.
(46) Zhao, Y.; Li, J.; Zhang, S.; Wang, X. Amidoxime-functionalized magnetic mesoporous silica for selective sorption of U(VI). *RSC Adv.* **2014**, *4* (62), 32710−32717.
(47) Manzoor, Q.; Sajid, A.; Hussain, T.; Iqbal, M.; Abbas, M.; Nisar, J. Efficiency of immobilized Zea mays biomass for the adsorption of chromium from simulated media and tannery wastewater. *J. Mater. Res. Technol.* **2019**, *8* (1), 75−86.
(48) Liu, F.; Zhou, K.; Chen, Q.; Wang, A.; Chen, W. Application of magnetic ferrite nanoparticles for removal of Cu(II) from copper-ammonia wastewater. *J. Alloys Compd.* **2019**, *773*, 140−149.
(49) Yuan, F.; Wu, C.; Cai, Y.; Zhang, L.; Wang, J.; Chen, L.; et al. Synthesis of phytic acid-decorated titanate nanotubes for high efficient and high selective removal of U(VI). *Chem. Eng. J.* **2017**, *322*, 353−365.
(50) Zeng, F.; He, Y.; Lian, Z.; Xu, J. The impact of solution chemistry of electrolyte on the sorption of pentachlorophenol and phenanthrene by natural hematite nanoparticles. *Sci. Total Environ.* **2014**, *466-467*, 577−585.
(51) French, R. A.; Jacobson, A. R.; Kim, B.; Isley, S. L.; Penn, L.; Baveye, P. C. Influence of ionic strength, pH, and cation valence on aggregation kinetics of titanium dioxide nanoparticles. *Environ. Sci. Technol.* **2009**, *43* (5), 1354−1359.
(52) Zhao, G.; Li, J.; Ren, X.; Chen, C.; Wang, X. Few-layered graphene oxide nanosheets as superior sorbents for heavy metal ion pollution management. *Environ. Sci. Technol.* **2011**, *45* (24), 10454−10462.
(53) Liu, X.; Li, J.; Wang, X.; Chen, C.; Wang, X. High performance of phosphate-functionalized graphene oxide for the selective adsorption of U(VI) from acidic solution. *J. Nucl. Mater.* **2015**, *466*, 56−64.
(54) Song, S.; Zhang, S.; Huang, S.; Zhang, R.; Yin, L.; Hu, Y.; et al. A novel multi-shelled Fe3O4@MnOx hollow microspheres for immobilizing U(VI) and Eu(III). *Chem. Eng. J.* **2019**, *355*, 697−709.
(55) Wang, T.; Liu, W.; Xiong, L.; Xu, N.; Ni, J. Influence of pH, ionic strength and humic acid on competitive adsorption of Pb(II), Cd(II) and Cr(III) onto titanate nanotubes. *Chem. Eng. J.* **2013**, *215-216*, 366−374.
(56) Meng, C.; Du, M. Y.; Zhang, Z. B.; et al. Open-Framework Vanadate as Efficient Ion Exchanger for Uranyl Removal. *Environ. Sci. Technol.* **2024**, *58* (21), 9456−9465.
(57) Kim, J.; Tsouris, C.; Oyola, Y.; Janke, C. J.; Mayes, R. T.; Dai, S.; et al. Uptake of uranium from seawater by amidoxime-based polymeric adsorbent: Field experiments, modeling, and updated economic assessment. *Ind. Eng. Chem. Res.* **2014**, *53* (14), 6076−6083.
(58) Kaur, S.; Rani, S.; Mahajan, R. K.; Asif, M.; Gupta, V. K. Synthesis and adsorption properties of mesoporous material for the removal of dye safranin: Kinetics, equilibrium, and thermodynamics. *J. Ind. Eng. Chem.* **2015**, *22*, 19−27.
(59) Liu, Y.; Wang, W.; Wang, A. Adsorption of lead ions from aqueous solution by using carboxymethyl cellulose-g-poly (acrylic acid)/attapulgite hydrogel composites. *Desalination* **2010**, *259*, 258−264.
(60) Langmuir, I. The constitution and fundamental properties of solids and liquids. Part I. Solids. *J. Am. Chem. Soc.* **1916**, *38*, 2221−2295.
(61) Rahman, M. S.; Islam, M. R. Effects of pH on isotherms modeling for Cu(II) ions adsorption using maple wood sawdust. *Chem. Eng. J.* **2009**, *149* (1−3), 273−280.
(62) Zhao, D.; Gao, X.; Chen, S.; Xie, F.; Feng, S.; Alsaedi, A.; Hayat, T.; Chen, C. Interaction between U(VI) with sulfhydryl groups functionalized graphene oxides investigated by batch and spectroscopic techniques. *J. Colloid Interface Sci.* **2018**, *524*, 129−138.
(63) Lu, S.; Zhu, H.; Gao, H.; Meng, Y.; Chen, C. Fabrication of sodium titanate nanospheres as efficient sorbent for the removal of U(VI) from aqueous solution. *J. Mol. Liq.* **2017**, *225*, 101−106.
(64) Zhuang, S.; Cheng, R.; Kang, M.; Wang, J. Kinetic and equilibrium of U(VI) adsorption onto magnetic amidoxime-functionalized chitosan beads. *J. Cleaner Prod.* **2018**, *188*, 655−661.
(65) Wang, Y.; Gu, Z.; Yang, J.; Liao, J.; Yang, Y.; Liu, N.; Tang, J. Amidoxime-grafted multiwalled carbon nanotubes by plasma techniques for efficient removal of uranium(VI). *Appl. Surf. Sci.* **2014**, *320*, 10−20.
(66) Xiong, L.; Chen, C.; Chen, Q.; Ni, J. Adsorption of Pb (II) and Cd (II) from aqueous solutions using titanate nanotubes prepared via hydrothermal method. *J. Hazard. Mater.* **2011**, *189* (3), 41−748.
(67) El-Rahman, K. M. A.; El-Kamash, A. M.; El-Sourougy, M. R.; Abdel-Moniem, N. M. Thermodynamic modeling for the removal of Cs^{+}, Sr^{2+}, $Ca^{2+}$and Mg^{2+} ions from aqueous waste solutions using zeolite A. *J. Radioanal. Nucl. Chem.* **2006**, *268* (2), 221−230.
(68) Zhu, Y.; Chen, T.; Liu, H.; Xu, B.; Xie, J. Kinetics and thermodynamics of Eu(III) and U(VI) adsorption onto palygorskite. *J. Mol. Liq.* **2016**, *219*, 272−278.
(69) Ding, C.; Cheng, W.; Sun, Y.; Wang, X. Novel fungus-Fe_3O_4 bio-nanocomposites as high performance adsorbents for the removal of radionuclides. *J. Hazard. Mater.* **2015**, *295*, 127−137.
(70) Rahchamani, J.; Mousavi, H. Z.; Behzad, M. Adsorption of methyl violet from aqueous solution by polyacrylamide as an adsorbent: Isotherm and kinetic studies. *Desalination* **2011**, *267* (2−3), 256−260.
(71) Zhu, J.; Liu, Q.; Li, Z.; Liu, J.; Zhang, H.; Li, R.; Wang, J. Efficient extraction of uranium from aqueous solution using an amino-functionalized magnetic titanate nanotubes. *J. Hazard. Mater.* **2018**, *353*, 9−17.
(72) Kanatzidis, M. G.; Fard, Z. H.; Malliakas, C. D.; et al. Selective Removal of Cs^{+}, Sr^{2+}, and Ni^{2+} by $K_{2x}Mg_xSn_{3-x}S_6$ (x = 0.5−1) (KMS-2) relevant to nuclear waste remediation. *Chem. Mater.* **2013**, *25* (10), 2116−2127.
(73) Sangvanich, T.; Sukwarotwat, V.; Wiacek, R. J.; Grudzien, R. M.; Fryxell, G. E.; Addleman, R. S.; Timchalk, C.; Yantasee, W. Selective capture of cesium and thallium from natural waters and simulated wastes with copper ferrocyanide functionalized mesoporous silica. *J. Hazard. Mater.* **2010**, *182* (1−3), 225−231.
(74) Manos, M. J.; Kanatzidis, M. G. Layered metal sulfides capture uranium from seawater. *J. Am. Chem. Soc.* **2012**, *134* (39), 16441−16446.
(75) Reich, T.; Foerstendorf, H.; Geipel, G.; Bernhard, G.; Massanek, A. Spectroscopic Characterization of the Uranium Carbonate Andersonite $Na_2Ca[UO_2(CO_3)_3]\cdot 6H_2O$. *Environ. Sci. Technol.* **2004**, *8* (22), 6032−6036.
(76) He, J.; Lu, Y.; Luo, G. Ca(II) imprinted chitosan microspheres: An effective and green adsorbent for the removal of Cu(II), Cd(II) and Pb(II) from aqueous solutions. *Chem. Eng. J.* **2014**, *244*, 202−208.

https://doi.org/10.1021/acsomega.4c05253
ACS Omega 2024, 9, 49108−49120